ACS APPLIED ENERGY MATERIALS

www.acsaem.org Letter

Different Photostability of $BiVO_4$ in Near-pH-Neutral Electrolytes

Siyuan Zhang,* Ibbi Ahmet, Se-Ho Kim, Olga Kasian, Andrea M. Mingers, Patrick Schnell, Moritz Kölbach, Joohyun Lim, Anna Fischer, Karl J. J. Mayrhofer, Serhiy Cherevko, Baptiste Gault, Roel van de Krol,* and Christina Scheu*

Cite This: *ACS Appl. Energy Mater.* 2020, 3, 9523−9527 Read Online

ACCESS | Metrics & More | Article Recommendations | Supporting Information

ABSTRACT: Photoelectrochemical water splitting is a promising route to produce hydrogen from solar energy. However, corrosion of photoelectrodes remains a fundamental challenge for their implementation. Here, we reveal different dissolution behaviors of $BiVO_4$ photoanode in pH-buffered borate, phosphate, and citrate (hole-scavenger) electrolytes, studied *in operando* employing an illuminated scanning flow cell. We demonstrate that decrease in photocurrents alone does not reflect the degradation of photoelectrodes. Changes in dissolution rates correlate to the evolution of surface chemistry and morphology. The correlative measurements on both sides of the liquid−semiconductor junction provide quantitative comparison and mechanistic insights into the degradation processes.

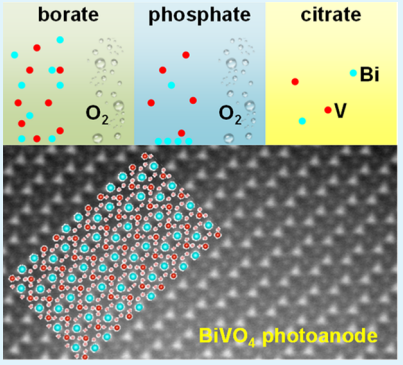

KEYWORDS: *Photoelectrochemical water splitting, bismuth vanadate, photocorrosion, illuminated scanning flow cell, aberration-corrected electron microscopy, atom probe tomography*

Photoelectrochemical (PEC) water splitting is a promising technology to harvest solar energy and store it directly as H_2 fuel.[1−4] A semiconducting photoelectrode functions both as a solar absorber and as an electrode that drives a half-cell reaction. Many solar absorbers developed in the photovoltaic industry, e.g., Si, III−V, II−VI, and halide perovskite compounds, have been integrated into PEC devices.[1−4] Direct contact of these materials with water, however, must be avoided to protect them from anodic corrosion and associated degradation. This motivates ongoing developments of corrosion-resistant metal oxide semiconductors as photoanodes for the oxygen evolution reaction (OER).[5−8] Thus far, $BiVO_4$ has been established as one of the best performing photoanode materials,[9−14] with reported photocurrents approaching its theoretical limit of 7.5 mA cm^{-2} under AM1.5G illumination.[14]

Although metal oxide semiconductors are much more stable in water than the conventional semiconductors mentioned above, few candidates have shown stability beyond a thousand hours.[12,15,16] The calculated Pourbaix diagram shows that $BiVO_4$ is stable for a wide range of potentials in near-pH-neutral solutions $4 < pH < 11$.[17] Therefore, $BiVO_4$ photoanodes have been mostly developed for operation in borate and phosphate electrolytes, with good buffer capacity at pH ∼9 and pH ∼7, respectively. Nevertheless, light-driven degradation of $BiVO_4$ in near-neutral electrolytes has been reported.[10,18] Under illumination, the quasi Fermi level of holes shifts to more anodic potentials, which can trigger additional anodic reactions (including the OER) and redefine the stability of photoanodes.[19−22] Experimental evidence on stoichiometric $BiVO_4$ dissolution was first documented in phosphate electrolytes using inductively coupled plasma mass spectrometry (ICPMS).[17] In another study, V was found to primarily leach out to borate electrolytes from $BiVO_4$ (note that the photoanode was covered by an OER catalyst layer).[13] To understand the different phenomena behind photocorrosion of $BiVO_4$, we present here *in operando* measurements to shed light on (1) the corrosion behaviors in different electrolytes, (2) the correlation between the corrosion and OER kinetics, and (3) the sensitivity of corrosion rates to the surface of $BiVO_4$.

To measure the corrosion rates *in operando*, we couple the ICPMS with an illuminated scanning flow cell (SFC) to enable fresh electrolytes continuously flowing over the $BiVO_4$ surface.[23] Thin (∼90 nm) and compact $BiVO_4$ films were prepared by pulsed laser deposition (PLD),[24] and pH-buffered borate, phosphate, and citrate electrolytes were respectively introduced through the SFC. As shown in Figure 1a, cyclic voltammetry (CV) scans on $BiVO_4$ enabled simultaneous

Received: August 7, 2020
Accepted: October 2, 2020
Published: October 6, 2020

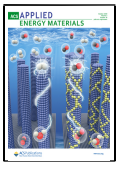

https://dx.doi.org/10.1021/acsaem.0c01904
ACS Appl. Energy Mater. 2020, 3, 9523−9527

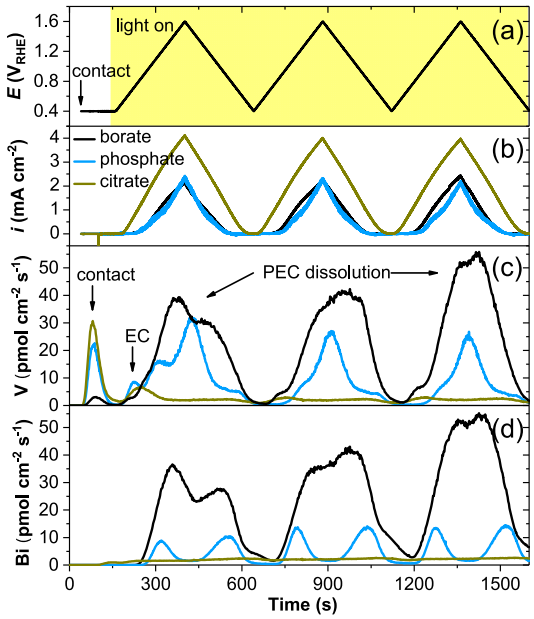

Figure 1. Time profiles of (a) applied potential to $BiVO_4$ against the reversible hydrogen electrode (RHE) scale (duration under illumination is highlighted in yellow), (b) the current density *i*, and (c) V and (d) Bi dissolution rates in borate, phosphate, and citrate.

evaluation of its activity (photocurrent density in Figure 1b), stability (dissolution curves in Figure 1c, d), and their dependence on the applied potential. The photocurrents in phosphate and borate electrolytes are similar, whereas the photocurrent in the hole-scavenging citrate electrolyte is higher due to the faster citrate oxidation reaction than OER. The corresponding CV scans without illumination (Figure S1) show negligible dark currents in all three electrolytes.

Different dissolution rates in three electrolytes are evident in Figure 1c,d. During the first CV cycle, $BiVO_4$ is dissolved at ~18, 6, and 2 pmol cm^{-2} s^{-1} in borate, phosphate, and citrate, respectively (1 pmol cm^{-2} s^{-1} translates to dissolution of 1.9 nm $BiVO_4$ per hour). To compare, little dissolution is observed without illumination after transient V dissolution upon contact with the electrolyte (Figure S1). The same transient dissolution peaks are labeled as "contact" and "EC" (electrochemical) dissolution in Figure 1c. Bi and V dissolution after 300 s, referred to as "PEC dissolution", are only observed under illumination.

The PEC dissolution peaks repeat during consecutive CV cycles, but their profiles are significantly different for the three electrolytes, as shown in Figure 1 and Figure S2 (replot of Figure 1 versus the potential). In borate, V and Bi dissolve simultaneously and reach their maxima at 1.6 and 1.2 V_{RHE} during the respective anodic and cathodic scans. In phosphate, V dissolution peaks at ~1.6 V_{RHE}, whereas Bi dissolution peaks at 1.1 and 0.8 V_{RHE} in the respective anodic and cathodic scans. In citrate, the dissolution rates hardly vary between 0.4 and 1.6 V_{RHE}.

Around neutral pH, buffer ligands are the major ion species in the electrolytes with concentrations $>10^{-2}$ M ($[OH^-] < 10^{-4}$ M for pH < 10) and therefore have a deciding influence on the stability of $BiVO_4$. Hole-scavenging citrate promotes the oxidation kinetics (photocurrent onset <0.4 V_{RHE}) so that the slower photocorrosion reactions (e.g., Bi^{3+} oxidation) are kept at constant rates.[23] In comparison to citrate oxidation, the photocurrent onset potentials for OER in borate and phosphate electrolytes are more anodic, ~0.8 V_{RHE}, and closely correlate to the onsets of the dissolution peaks. Therefore, the PEC dissolution in borate and phosphate can be kinetically coupled to the OER, a kinetically demanding reaction known for driving dissolution of many anode materials, including the more stable IrO_2.[25]

In phosphate solutions, Bi dissolution slows down at more anodic potentials whereas V dissolution keeps increasing (Figure 1c,d) . This suggests that the $BiVO_4$ surface becomes Bi-rich at higher anodic potentials, before Bi is further dissolved in the subsequent cathodic scan. The presence of a Bi-rich layer has been hypothesized,[10] and recently observed on a $BiVO_4$ surface immersed in phosphate by ambient pressure hard X-ray photoelectron spectroscopy, evidencing $BiPO_4$ formation under illumination and its dissolution in the dark.[26]

In borate solutions, dissolution was only reported *ex situ* on $BiVO_4$ covered by FeOOH/NiOOH catalysts, exemplifying enhanced OER kinetics and lower dissolution of primarily V.[13] In contrast, we find that the bare $BiVO_4$ surface has poor stability during OER in borate, showing the highest dissolution rates among the three studied electrolytes. Furthermore, as shown in Figure 1c,d), the dissolution rates in borate keep increasing from the first to the third CV cycle.

The changing dissolution rates are also monitored in an accelerated degradation test shown in Figure 2, as most of the

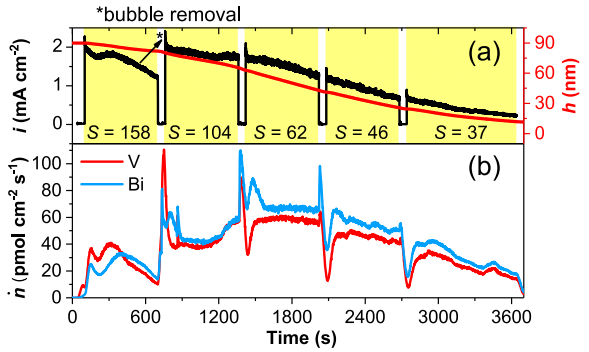

Figure 2. Time profiles of (a) photocurrent density *i*, film thickness *h*, and (b) dissolution rates $\dot{n}$ of $BiVO_4$ held at 1.6 V_{RHE} in borate. The duration under illumination is highlighted in yellow, with calculated stability number *S* shown in each illumination cycle.

examined $BiVO_4$ photoanode dissolved within 1 h of OER at 1.6 V_{RHE}. Throughout the life cycle, the dissolution rates first increased to ~60 pmol cm^{-2} s^{-1}, then decreased with time toward zero. The amount of dissolved material is determined by integration, which enables a reconstruction of the film thickness with time (right vertical axis in Figure 2a). A drop in the photocurrent during the first illumination cycle recovered after pausing the measurement, during which the SFC was detached from the $BiVO_4$ surface and then approached back to remove evolved O_2 bubbles from the surface. Such breaks were introduced three more times during the chronoamperometric measurement.

Varying dissolution rates can be correlated to chemical composition and morphology of $BiVO_4$ photoanodes, characterized before and after OER. X-ray photoelectron spectroscopy (XPS) reveals that as-synthesized $BiVO_4$ films have a V-rich surface (V atomic concentration 59 ± 1%), which correlates to the transient dissolution of primarily V amounting

https://dx.doi.org/10.1021/acsaem.0c01904
ACS Appl. Energy Mater. 2020, 3, 9523−9527

to ~2 nmol cm^{-2} (Figures 1 and S1). After ~20 min OER, the surface becomes close to stoichiometry (V atomic concentration 51 ± 2%), on which stoichiometric PEC dissolution proceeded in borate.

As shown in Figure 3a, as-synthesized $BiVO_4$ films are composed of crystallites with lateral sizes of 200−500 nm. The

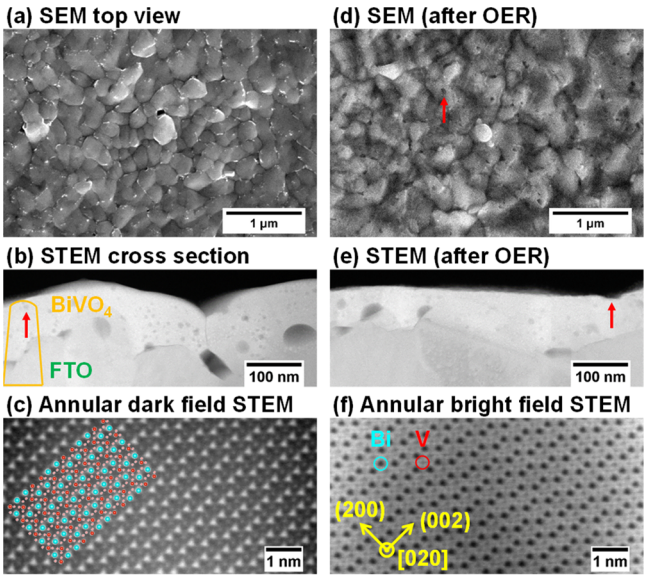

Figure 3. Morphology of $BiVO_4$ films (a,b) before and (c−f) after 20 min OER in borate. (a,d) Top view scanning electron microscopy (SEM), (b,e) cross-section view scanning transmission electron microscopy (STEM), and (c,f) atomically resolved STEM micrographs with overlaid monoclinic scheelite $BiVO_4$ structure.

surface becomes porous after OER in borate: The arrow in Figure 3d points to a pore, while cross-section images (Figure 3b,e) reveal porous features throughout the thickness of the film. As photocorrosion progresses, the once embedded pores emerge to the surface (arrow in Figure 3e), while the $BiVO_4$ film remains as the monoclinic scheelite phase (Figure 3c,f). The porous morphology causes the effective surface area to increase, which explains the initial increase in the dissolution rates. Dissolution stops at the end of the 1 h measurement, and Figure S4 shows that little $BiVO_4$ remains within the exposed area.

Larger pores in the cross-section images (Figure 3b,e) are present along the interface between $BiVO_4$ and fluorine-doped SnO_2 (FTO) substrate. The high surface roughness of FTO and limited surface diffusion of deposited species during room temperature PLD growth may explain the porosity. We also observe smaller (~10 nm), round-shaped dark features, whose composition is further examined by atom probe tomography (APT). A needle-shaped APT sample across the FTO/$BiVO_4$ interface is shown in Figure 4a. One of the small spherical features is highlighted in Figure 4b, which the APT analysis determines as V-rich oxide, as it contains fewer Bi atoms (Figure 4c). We postulate that as PEC dissolution exposes such V-rich oxides to the surface, they are unstable in aqueous electrolytes[23] and their preferential dissolution would lead to a porous surface.

A decrease in the photocurrent with time is conventionally used as the indicator for photocorrosion.[10,13,17,18] For photoanodes, both the OER and the anodic corrosion reaction are driven by photogenerated holes. However, as shown in

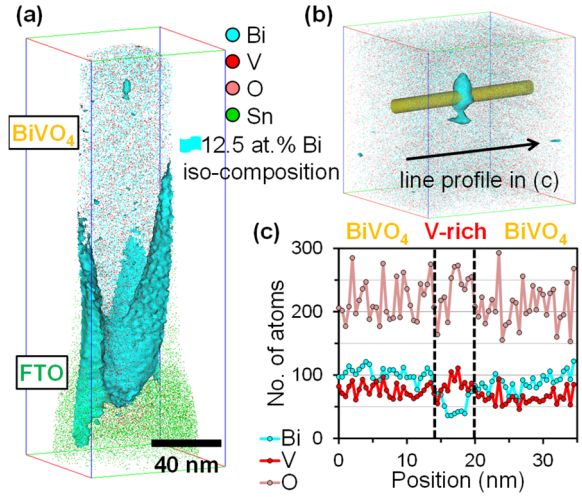

Figure 4. (a) 3D atom map of a needle-shaped APT sample from a similar region as the yellow outline in Figure 3b, (b) sectioned volume with a cylindrical Φ4.3 × 35 nm^3 region across a feature enveloped by the iso-composition surface of 12.5 at. % Bi, and (c) detected numbers of Bi, V, O atoms within the cylinder.

Figure 2, the steady-state photocurrents vary little between the first two illumination cycles, even though by this point one-third of the film is dissolved (from 90 to 60 nm). This can be explained by the limited carrier diffusion length of $BiVO_4$ (~70 nm),[27,28] in which holes generated in the first 70 nm of the film are able to contribute to the photocurrent statistically. As a result, the photocurrent density does not decrease during the initial photocorrosion of thicker films. Below the observed transition at ~60 nm (from the third illumination cycle in Figure 2), which is indeed close to the carrier diffusion length of $BiVO_4$, the surface hole population becomes limited by the absorber volume, leading to decreasing photocurrents and dissolution rates.

We further evaluate the relative stability of $BiVO_4$ with respect to the OER, using the stability number S, a quantity introduced for Ir-based OER catalysts as the ratio between numbers of evolved O_2 molecules and dissolved metal atoms in the electrolyte.[25] As shown in Figure 2, the relative stability drops monotonically from S = 158 averaged over the first illumination cycle to S = 37 during the fifth. In comparison, WO_3 photoanodes studied in sulfuric acid have similar S numbers, ranging from 100 to 200,[29] whereas OER anodes of commercial polymer electrolyte membrane electrolyzers made of iridium compounds are remarkably more stable, with S = 10^4−10^7.[25] Having S well over unity indicates that the OER is the main anodic reaction, which could kinetically inhibit photocorrosion.[19] However, with S on the order of 10^2, bare $BiVO_4$ surfaces only demonstrate ~1 h lifetime in the borate buffer. The lifetime of an electrode is proportional to S and the loading (film thickness).[25] Since $BiVO_4$ photoanodes must remain thin (~100 nm) in order to ensure efficient carrier collection,[27,28] they need to have S numbers on the order of 10^6 in order to reach the >10^4 h lifetime required for practical applications. We demonstrate that kinetic inhibition by citrate oxidation only slows down the dissolution by 1 order of magnitude. Therefore, passivating layers including OER catalysts are indispensable to protect $BiVO_4$ surface from photocorrosion, having thus far demonstrated stable operation for 1100 and 500 h.[12,13]

https://dx.doi.org/10.1021/acsaem.0c01904
ACS Appl. Energy Mater. 2020, 3, 9523−9527

In summary, using illuminated SFC coupled to ICPMS, we compared dissolution behaviors of $BiVO_4$ during light-driven OER in three pH-buffered electrolytes. Bi and V dissolve at different potential ranges in phosphate, whereas their dissolution in borate is synchronous. Photocurrents alone cannot reflect the progression of photocorrosion, especially for thicker photoabsorbers with limited carrier diffusion lengths. Therefore, we propose to rely on *in operando* dissolution measurements to evaluate photostability. The PEC dissolution rates are sensitive to the surface chemistry and morphology of $BiVO_4$. As photocorrosion progresses, nanoscopic V-rich oxides found within the $BiVO_4$ film are exposed to the electrolyte and preferentially dissolved, leading to accelerated corrosion. The toolset to characterize both sides of the semiconductor−liquid junction can facilitate future investigations to develop protection strategies against photocorrosion.

■ ASSOCIATED CONTENT

Supporting Information

The Supporting Information is available free of charge at https://pubs.acs.org/doi/10.1021/acsaem.0c01904.

Experimental details, controlled electrochemical experiments in the dark, analysis of photoelectrochemical results, X-ray photoelectron spectroscopy, scanning electron microscopy, and atom probe tomography characterization (PDF)

■ AUTHOR INFORMATION

Corresponding Authors

Siyuan Zhang − *Max-Planck-Institut für Eisenforschung GmbH, 40237 Düsseldorf, Germany;* orcid.org/0000-0001-7045-0865; Email: siyuan.zhang@mpie.de

Roel van de Krol − *Institute for Solar Fuels, Helmholtz-Zentrum Berlin für Materialien und Energie GmbH, 14109 Berlin, Germany;* orcid.org/0000-0003-4399-399X; Email: roel.vandekrol@helmholtz-berlin.de

Christina Scheu − *Max-Planck-Institut für Eisenforschung GmbH, 40237 Düsseldorf, Germany;* orcid.org/0000-0001-7916-1533; Email: scheu@mpie.de

Authors

Ibbi Ahmet − *Institute for Solar Fuels, Helmholtz-Zentrum Berlin für Materialien und Energie GmbH, 14109 Berlin, Germany;* orcid.org/0000-0003-0986-1950

Se-Ho Kim − *Max-Planck-Institut für Eisenforschung GmbH, 40237 Düsseldorf, Germany*

Olga Kasian − *Max-Planck-Institut für Eisenforschung GmbH, 40237 Düsseldorf, Germany; Helmholtz-Zentrum Berlin GmbH, Helmholtz Institut Erlangen-Nürnberg, 14109 Berlin, Germany;* orcid.org/0000-0001-6315-0637

Andrea M. Mingers − *Max-Planck-Institut für Eisenforschung GmbH, 40237 Düsseldorf, Germany*

Patrick Schnell − *Institute for Solar Fuels, Helmholtz-Zentrum Berlin für Materialien und Energie GmbH, 14109 Berlin, Germany*

Moritz Kölbach − *Max-Planck-Institut für Eisenforschung GmbH, 40237 Düsseldorf, Germany;* orcid.org/0000-0003-1828-0437

Joohyun Lim − *Max-Planck-Institut für Eisenforschung GmbH, 40237 Düsseldorf, Germany; Department of Chemistry, Kangwon National University, Chuncheon 24341, Republic of Korea;* orcid.org/0000-0003-3880-2634

Anna Fischer − *Institute of Inorganic and Analytical Chemistry, University of Freiburg, 79104 Freiburg, Germany*

Karl J. J. Mayrhofer − *Helmholtz Institut Erlangen-Nürnberg for Renewable Energy (IEK-11), Forschungszentrum Jülich, 91058 Erlangen, Germany*

Serhiy Cherevko − *Helmholtz Institut Erlangen-Nürnberg for Renewable Energy (IEK-11), Forschungszentrum Jülich, 91058 Erlangen, Germany*

Baptiste Gault − *Max-Planck-Institut für Eisenforschung GmbH, 40237 Düsseldorf, Germany; Department of Materials, Royal School of Mines, Imperial College London, London SW7 2AZ, United Kingdom*

Complete contact information is available at: https://pubs.acs.org/10.1021/acsaem.0c01904

Notes

The authors declare no competing financial interest.

■ ACKNOWLEDGMENTS

S.Z. and C.S. acknowledge funding from the German Research Foundation (DFG). J.L. acknowledges financial support from the Alexander von Humboldt Foundation. B.G. and S.H.K. acknowledge financial support from the ERC-CoG-SHINE-771602.

■ REFERENCES

(1) Khaselev, O.; Turner, J. A. A Monolithic Photovoltaic-Photoelectrochemical Device for Hydrogen Production via Water Splitting. *Science* **1998**, *280*, 425−427.

(2) Grätzel, M. Photoelectrochemical Cells. *Nature* **2001**, *414*, 338−344.

(3) Ager, J. W.; Shaner, M. R.; Walczak, K. A.; Sharp, I. D.; Ardo, S. Experimental Demonstrations of Spontaneous, Solar-Driven Photoelectrochemical Water Splitting. *Energy Environ. Sci.* **2015**, *8*, 2811−2824.

(4) Zhang, K.; Ma, M.; Li, P.; Wang, D. H.; Park, J. H. Water Splitting Progress in Tandem Devices: Moving Photolysis beyond Electrolysis. *Adv. Energy Mater.* **2016**, *6*, 1600602.

(5) Kudo, A.; Miseki, Y. Heterogeneous Photocatalyst Materials for Water Splitting. *Chem. Soc. Rev.* **2009**, *38*, 253−278.

(6) Sivula, K.; van de Krol, R. Semiconducting Materials for Photoelectrochemical Energy Conversion. *Nat. Rev. Mater.* **2016**, *1*, 15010.

(7) He, Y.; Hamann, T.; Wang, D. Thin Film Photoelectrodes for Solar Water Splitting. *Chem. Soc. Rev.* **2019**, *48*, 2182−2215.

(8) Lee, D. K.; Lee, D.; Lumley, M. A.; Choi, K.-S. Progress on Ternary Oxide-Based Photoanodes for Use in Photoelectrochemical Cells for Solar Water Splitting. *Chem. Soc. Rev.* **2019**, *48*, 2126−2157.

(9) Kudo, A.; Omori, K.; Kato, H. A Novel Aqueous Process for Preparation of Crystal Form-Controlled and Highly Crystalline $BiVO_4$ Powder from Layered Vanadates at Room Temperature and Its Photocatalytic and Photophysical Properties. *J. Am. Chem. Soc.* **1999**, *121*, 11459−11467.

(10) Sayama, K.; Nomura, A.; Arai, T.; Sugita, T.; Abe, R.; Yanagida, M.; Oi, T.; Iwasaki, Y.; Abe, Y.; Sugihara, H. Photoelectrochemical Decomposition of Water into H_2 and O_2 on Porous $BiVO_4$ Thin-Film Electrodes under Visible Light and Significant Effect of Ag Ion Treatment. *J. Phys. Chem. B* **2006**, *110*, 11352−11360.

(11) Park, Y.; McDonald, K. J.; Choi, K.-S. Progress in Bismuth Vanadate Photoanodes for Use in Solar Water Oxidation. *Chem. Soc. Rev.* **2013**, *42*, 2321−2337.

(12) Kuang, Y.; Jia, Q.; Ma, G.; Hisatomi, T.; Minegishi, T.; Nishiyama, H.; Nakabayashi, M.; Shibata, N.; Yamada, T.; Kudo, A.; Domen, K. Ultrastable Low-Bias Water Splitting Photoanodes via Photocorrosion Inhibition and in situ Catalyst Regeneration. *Nature Energy* **2017**, *2*, 16191.

(13) Lee, D. K.; Choi, K.-S. Enhancing Long-Term Photostability of $BiVO_4$ Photoanodes for Solar Water Splitting by Tuning Electrolyte Composition. *Nature Energy* **2018**, *3*, 53−60.
(14) Kim, J. H.; Lee, J. S. Elaborately Modified $BiVO_4$ Photoanodes for Solar Water Splitting. *Adv. Mater.* **2019**, *31*, 1806938.
(15) Nandjou, F.; Haussener, S. Degradation in Photoelectrochemical Devices: Review with an Illustrative Case Study. *J. Phys. D: Appl. Phys.* **2017**, *50*, 124002.
(16) Bae, D.; Seger, B.; Vesborg, P. C. K.; Hansen, O.; Chorkendorff, I. Strategies for Stable Water Splitting via Protected Photoelectrodes. *Chem. Soc. Rev.* **2017**, *46*, 1933−1954.
(17) Toma, F. M.; Cooper, J. K.; Kunzelmann, V.; McDowell, M. T.; Yu, J.; Larson, D. M.; Borys, N. J.; Abelyan, C.; Beeman, J. W.; Yu, K. M.; Yang, J.; Chen, L.; Shaner, M. R.; Spurgeon, J.; Houle, F. A.; Persson, K. A.; Sharp, I. D. Mechanistic Insights into Chemical and Photochemical Transformations of Bismuth Vanadate Photoanodes. *Nat. Commun.* **2016**, *7*, 12012.
(18) Berglund, S. P.; Flaherty, D. W.; Hahn, N. T.; Bard, A. J.; Mullins, C. B. Photoelectrochemical Oxidation of Water Using Nanostructured $BiVO_4$ Films. *J. Phys. Chem. C* **2011**, *115*, 3794−3802.
(19) Gerischer, H. On the Stability of Semiconductor Electrodes against Photodecomposition. *J. Electroanal. Chem. Interfacial Electrochem.* **1977**, *82*, 133−143.
(20) Chen, S.; Wang, L.-W. Thermodynamic Oxidation and Reduction Potentials of Photocatalytic Semiconductors in Aqueous Solution. *Chem. Mater.* **2012**, *24*, 3659−3666.
(21) Hu, S.; Lewis, N. S.; Ager, J. W.; Yang, J.; McKone, J. R.; Strandwitz, N. C. Thin-Film Materials for the Protection of Semiconducting Photoelectrodes in Solar-Fuel Generators. *J. Phys. Chem. C* **2015**, *119*, 24201−24228.
(22) Eichhorn, J.; Liu, G.; Toma, F. M. in *Integrated Solar Fuel Generators*, Sharp, I. D.; Atwater, H. A.; Lewerenz, H.-J., Eds.; The Royal Society of Chemistry, 2019; pp 281−303. DOI: 10.1039/9781788010313-00281.
(23) Zhang, S.; Rohloff, M.; Kasian, O.; Mingers, A. M.; Mayrhofer, K. J. J.; Fischer, A.; Scheu, C.; Cherevko, S. Dissolution of $BiVO_4$ Photoanodes Revealed by Time-Resolved Measurements under Photoelectrochemical Conditions. *J. Phys. Chem. C* **2019**, *123*, 23410−23418.
(24) Kölbach, M.; Harbauer, K.; Ellmer, K.; van de Krol, R. Elucidating the Pulsed Laser Deposition Process of $BiVO_4$ Photoelectrodes for Solar Water Splitting. *J. Phys. Chem. C* **2020**, *124*, 4438−4447.
(25) Geiger, S.; Kasian, O.; Ledendecker, M.; Pizzutilo, E.; Mingers, A. M.; Fu, W. T.; Diaz-Morales, O.; Li, Z.; Oellers, T.; Fruchter, L.; Ludwig, A.; Mayrhofer, K. J. J.; Koper, M. T. M.; Cherevko, S. The Stability Number as a Metric for Electrocatalyst Stability Benchmarking. *Nat. Catalysis* **2018**, *1*, 508−515.
(26) Favaro, M.; Abdi, F. F.; Lamers, M.; Crumlin, E. J.; Liu, Z.; van de Krol, R.; Starr, D. E. Light-Induced Surface Reactions at the Bismuth Vanadate/Potassium Phosphate Interface. *J. Phys. Chem. B* **2018**, *122*, 801−809.
(27) Abdi, F. F.; Savenije, T. J.; May, M. M.; Dam, B.; van de Krol, R. The Origin of Slow Carrier Transport in BiVO4 Thin Film Photoanodes: A Time-Resolved Microwave Conductive Study. *J. Phys. Chem. Lett.* **2013**, *4*, 2752−2757.
(28) Rettie, A. J. E.; Lee, H. C.; Marshall, L. G.; Lin, J.-F.; Capan, C.; Lindemuth, J.; McCloy, J. S.; Zhou, J.; Bard, A. J.; Mullins, C. B. Combined Charge Carrier Transport and Photoelectrochemical Characterization of $BiVO_4$ Single Crystals: Intrinsic Behavior of a Complex Metal Oxide. *J. Am. Chem. Soc.* **2013**, *135*, 11389−11396.
(29) Knöppel, J.; Zhang, S.; Speck, F. D.; Mayrhofer, K. J. J.; Scheu, C.; Cherevko, S. Time-Resolved Analysis of Dissolution Phenomena in Photoelectrochemistry − A Case Study of WO_3 Photocorrosion. *Electrochem. Commun.* **2018**, *96*, 53−56.

https://dx.doi.org/10.1021/acsaem.0c01904
ACS Appl. Energy Mater. 2020, 3, 9523−9527